Quantitative microscopic measurement of void distribution in shear bands in $Zr_{66.7}Cu_{33.3}$ metallic glass

A. C. Y. Liu,[1,*] D. M. Paganin,[1] L. Bourgeois,[2,3] P. N. H. Nakashima,[2,3,4]
R. T. Ott,[5] and M. J. Kramer[5,6]

[1]*School of Physics, Monash University, Clayton, 3800, Victoria, Australia.*
[2]*Monash Centre for Electron Microscopy, Monash University, Clayton, 3800, Victoria, Australia.*
[3]*Department of Materials Engineering, Monash University, Clayton, 3800, Victoria, Australia.*
[4]*Australian Research Council Centre of Excellence for Design in Light Metals, Monash University,
Clayton, 3800, Victoria, Australia.*
[5]*Division of Materials Sciences and Engineering, Ames Laboratory, Ames, Iowa, 50011, USA*
[6]*Department of Materials Science and Engineering, Iowa State University, Ames, Iowa, 50011, USA*

We employ an electron phase retrieval technique in the transmission electron microscope to reconstruct the projected thickness maps of metallic glass specimens and measure the void distribution at a microscopic level. We examine an as-spun melt-spun $Zr_{66.7}Cu_{33.3}$ glass and the shear bands formed in this glass from inhomogeneous deformation in tension and compression. Both as-spun and deformed glasses show no variation in projected thickness indicative of voids down to the limit of this medium-resolution technique (0.32 nm). This demonstrates that the free volume generated in deformation does not condense into stable voids larger than 0.32 nm in radius, but is distributed diffusely in shear bands.

PACS number(s): 61.43.Fs, 61.05.J−, 62.20.mj

I. INTRODUCTION

"Free volume," or the volume available for diffusive motion in a glass, is an important parameter to describe the dynamics of the glass transition[1] and the state of relaxation of the glass[2]. During deformation free volume is created[3] resulting in bulk density decreases of 0.1%–0.2%.[4] In the homogeneous regime, close to the glass transition temperature, and at low strain rate, this free volume is distributed uniformly. In contrast, in the inhomogeneous regime at low temperature and high strain rate, the free volume is generally thought to be localized in shear bands, the regions where the shear strain localizes.[3] The reason for the shear localization and the structure of the shear bands that form are outstanding questions, although the formation of shear bands has many ramifications for the ductility of the glass.[5] Bulk positron annihilation spectroscopy indicates that in inhomogeneously deformed glasses the free volume exists in three distinct populations: small tetrahedral holes, flow defects of approximately one atomic volume, and larger voids 2–2.7 Å in radius.[6]

Previous microscopic observations of shear bands in the transmission electron microscope (TEM) have suggested that 1-nm-sized voids form in shear bands due to the coalescence of free volume,[7–9] a finding that has some theoretical support.[10] In an early experiment, a small objective aperture was placed in the back focal plane to form a dark-field image from electrons scattered by nanometer-sized objects into low angles.[8] An increase in intensity in these dark-field images around cracks was ascribed to an increase in small-angle scattering from voids. However, the size of the un-diffracted beam in the TEM is finite, and the objective aperture in this case included electrons from the un-diffracted beam. Instead of imaging in a pure dark-field mode, these researchers were operating in a mode similar to Schlieren contrast, in which a knife-edge aperture is placed in the back focal plane and blocks electrons from half the diffraction plane.

Schlieren contrast mode has been used to enhance image contrast from phase objects such as biological specimens[11] and magnetic domains (in this case called Foucault imaging[12]). In this mode, the contrast is approximately proportional to the derivative in the phase shift taken perpendicular to the aperture edge.[13] At a crack, the electron phase shifts due to interaction with the material will change rapidly, giving rise to strips of bright and dark contrast parallel to the crack, for phase shifts decreasing and increasing with position, respectively, as observed in the early TEM images of shear bands. In this early study, the amount of bright contrast at the crack changed depending on in which direction the objective aperture was placed.[8] This observation is consistent with Schlieren mode contrast, and not low-angle scattering due to voids. Voids that are on average spherical would scatter equally into different azimuthal directions for a given magnitude of scattering vector, and would not give rise to a change in contrast for objective apertures placed in different directions.

Other TEM observations of voids in shear bands have employed an image filtering and intensity thresholding technique.[7,9] However, it has been demonstrated that the assumptions underlying the high-resolution TEM image analysis were not supported, giving rise to spurious detection of voids in thinner areas of the TEM specimen.[14] We will also demonstrate this in Sec. III. Given that previous observations of voids in shear bands are unreliable, a quantitative microscopic measurement of the void distribution in shear bands is desirable to clarify the structure of shear bands and their formation.

II. EXPERIMENTAL

We examine the distribution of voids in as-spun and inhomogeneously deformed $Zr_{66.7}Cu_{33.3}$ using a quantitative electron phase retrieval technique to reconstruct the specimen projected thickness map. The technique was originally

developed for x-ray phase contrast microscopy[15], and has been generalized to include spherically aberrated objective optics.[16] The technique applies to single-material objects in the strong phase and weak absorption regimes, and transforms a single out-of-focus phase contrast image to the projected thickness map of the specimen. This single image technique is ideal for examining materials in a fragile equilibrium such as glasses, or for *in situ* studies. The reconstruction transform is as follows:[16]

$$T(x,y) = -\frac{1}{\mu} \log_e \left(\mathcal{F}^{-1} \left\{ \frac{\mathcal{F}[I_\delta(x,y)/I_0]}{1 - \frac{2\pi\delta\lambda\sigma V_0}{\mu}(k_x^2 + k_y^2) - \frac{\pi C_s\lambda^3\sigma V_0}{\mu}(k_x^2 + k_y^2)^2} \right\} \right). \tag{1}$$

Here $T(x,y)$ is the projected thickness map, $\mathcal{F}$ denotes a two-dimensional (2D) Fourier transform, $I_\delta(x,y)$ is a phase contrast image taken at defocus δ, I_0 is the incident intensity, and k_x and k_y are spatial frequencies. λ, σ, and C_s are the electron wavelength, interaction constant, and spherical aberration coefficient, respectively. μ and V_0 are the linear attenuation coefficient and mean inner potential of the specimen. We estimated μ from the in-focus intensity of a region whose thickness was measured by tilting in the TEM and calculating the lateral displacement of surface features, yielding $\mu = 0.022 \pm 0.0004$ nm^{-1}. V_0 was estimated as $V_0 = 18.22$ V using an empirical rule to approximate bonding effects[17] and an atomic volume of 0.0195 nm^3.[18] The value for the defocus (optimal for this technique at -50 nm)[16] was measured by fitting the diffractogram, and the value of C_s employed was the nominal value of 1.0 mm. The transform takes a single phase contrast TEM image and applies a Fourier filter to reverse the effects of out-of-focus contrast to obtain the projected thickness map.[16] The resolution limit of the technique is the limit imposed by the approximations inherent in Eq. (1) and the image pixel size added in quadrature, yielding 0.32 nm or approximately 20 atomic volumes in this glass.[16] However, resolution must be discussed in the context of the object, a topic we return to in Sec. III.

The as-spun glasses were jet-polished to perforation (Tenupol 5, 33.3%:66.7% nitric acid:methanol, -40 °C, 12 V, 100 mA) and then ion milled to remove surface oxide (Gatan Precision Ion Polishing System, 5 min, 1 keV, LN_2, 2°). Specimens were deformed by bending the melt-spun ribbon over a razor blade to an angle of ~45°. These specimens were then jet-polished from one side to preserve the shear bands formed in compression and tension, and then ion milled. Similar to previous studies, the deformed specimens were prepared for TEM examination after the shear force was removed.[8,9] Other studies have thinned the specimen first and then examined areas near crack-tips that are assumed to correspond to shear bands that form from deformation during routine specimen handling.[7] It is evident that in the former case the structure of the shear bands may relax during the specimen preparation. However, the latter technique relies on *ad hoc* identification of shear bands based on preconceptions of the shear band contrast and appearance in the TEM. As will be demonstrated shortly, there is little ambiguity in our study about where the shear bands are located.

We have taken every precaution to avoid specimen heating and structural modification during specimen preparation. Specimens were examined within 24 h of preparation due to the propensity for surface oxide formation. TEM specimens were examined in a scanning electron microscope (JEOL JSM-7001F FEGSEM; 15 keV) to identify where shear bands would intersect with electron-transparent regions. Phase contrast TEM images were obtained on a JEOL JEM 2100F FEGTEM (200 keV) with a Gatan UltraScan 1000 (2048×2048) CCD camera. Prior to applying Eq. (1) the images were deconvolved by a modulation transfer function determined using the aperture method.[19] The algorithm was executed using fast Fourier transforms (FFTs) in interactive data language (IDL 7.0). Prior to the application of the transform, the input images were binned to 8 times coarser resolution and then zero-padded to twice their size, to avoid aliasing.

III. RESULTS AND DISCUSSION

In a phase contrast TEM image taken in negative defocus conditions, regions of charge density deficit, such as voids, appear bright. Based on this, previous studies have used an intensity thresholding analysis to support the presence of voids in shear bands. Contrast in a phase contrast image of an amorphous specimen arises from several sources. At low spatial frequencies there is amplitude, or mass thickness, contrast due to absorption. At higher spatial frequencies there is phase contrast from scattering and interference due to atomic density variations and regions of correlated atomic structure.[20] In previous work using intensity thresholding to detect voids, the intensity variations in the phase contrast image were attributed exclusively to atomic density variations, which would, to first approximation increase as $N^{1/2}$, where N is the number of atoms in a column of material with diameter equal to the instrument resolution. This implies that the intensity variations in a phase contrast image would increase as the sample increases in thickness.

In practice this does not occur, due to the component of phase contrast due to atomic clustering. Beams scattered from different atomic clusters within the same column can interfere destructively or constructively. As the thickness increases, and more clusters contribute, the intensity variation from column to column is decreased. This same mechanism is responsible for the reduction in intensity variance with increased thickness in dark-field images of amorphous specimens.[21] Thus, in phase contrast images of amorphous materials we expect that the intensity fluctuations due to phase contrast will decrease in magnitude at a thickness related to the degree and size of the regions of correlated atomic structure. Using intensity thresholding, a greater number of high-intensity pixels will
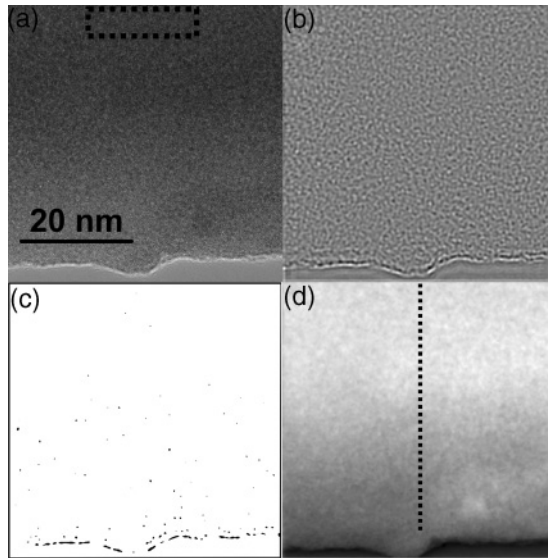
FIG. 1. (a) Phase contrast image of the as-spun specimen ($\delta = -180$ nm). (b) Image after annular Fourier filter is applied admitting $0.5 \leqslant |k| = \sqrt{k_x^2 + k_y^2} \leqslant 1.8$ nm^{-1}. (c) Thresholded image containing pixels with intensity grater than three standard deviations above the mean (inverted contrast). (d) Reconstructed projected thickness of area using Eq. (1).
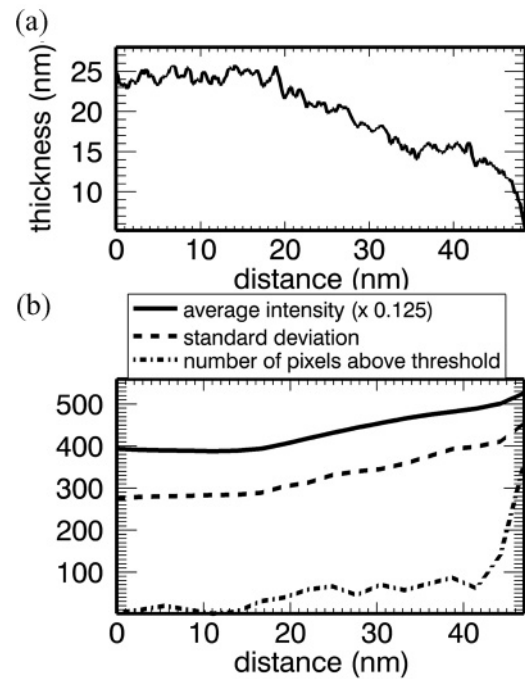

FIG. 2. (a) Profile of projected thickness shown in Fig. 1(d). (b) Average intensity ($\times 0.125$) and standard deviation in intensity distribution of rectangular regions (width $=25$ nm; height $=5$ nm) of the phase contrast image shown in Fig. 1(a). A distance of 0 nm corresponds to the top of the image. The corresponding number of nonzero pixels in the thresholded image is also shown (dot-dash line). Thinner regions of the specimen correspond to areas with greater intensity fluctuations in the phase contrast image and subsequently, more detected bright pixels in the thresholded image.

thus be detected in thinner regions of the specimen, making this technique unreliable for detecting voids when the specimen thickness changes appreciably.

Before detailing the main results of our experiment, we will replicate the intensity-thresholding analysis of previous studies and demonstrate explicitly its sensitivity to specimen thickness.[7,9] Figure 1(a) displays a phase contrast image of an as-spun specimen, taken at a defocus value of $\delta = -180$ nm, to transfer a large pass band of spatial frequencies around 1 nm^{-1} with the same contrast, given our experimental parameters. Figure 1(b) displays the same image after an annular Fourier filter admitting spatial frequencies $0.5 \leqslant |k| = \sqrt{k_x^2 + k_y^2} \leqslant 1.8$ nm^{-1} has been applied. This step removes absorption contrast from the image. We then applied a threshold to the image, only displaying pixels with intensity greater than three standard deviations above the mean, as shown in Fig. 1(c) (contrast inverted for clarity). Clearly, more pixels with an intensity above the threshold are detected in the thinner region of the specimen. We applied Eq. (1) to recover the projected thickness of this region of the specimen [Fig. 1(d)]. A profile through this projected thickness along the dotted line shown is displayed in Fig. 2(a) with a transverse distance of 0 nm corresponding to the top of the micrograph. In Fig. 2(b) we plot the average intensity and standard deviation in the intensity distribution from rectangular regions (width $=25$ nm and height $=5$ nm as shown in with dotted line) of the phase contrast image [Fig. 1(a)] centered along the profile at the distances shown. As the thickness of the specimen decreases, the average intensity and also variance in the intensity increase. We also plot the number of pixels in the filtered image with an intensity above the threshold from corresponding rectangular regions. Clearly, the number of pixels above the intensity threshold is a sensitive function of thickness. We note that the distance over which this analysis

was carried out avoids the edge of the specimen, and strong intensity variations due to the Fresnel fringes extending into vacuum.

The sensitivity of the Fourier filtering and intensity thresholding technique to specimen thickness and the fact that shear bands are generally thinner regions of the TEM specimen due to preferential thinning, or shearing,[7–9] makes this analysis unreliable for detecting voids. In contrast, the technique we employ in our study reverses the out-of-focus phase contrast in a single phase contrast TEM image to obtain quantitative specimen information in the form of the projected thickness. We then employ the autocorrelation function to detect the size of any variations in this projected thickness, for example, due to voids.[16]

Figure 3 shows SEM images of a typical deformed TEM specimen used in this study. The perforation has formed in the middle of the network of shear steps [Fig. 3(a)]. It is clear from the higher magnification image [Fig. 3(b)] that the shear bands have etched preferentially and that their position is clearly marked around the edge of the perforation at the apex of the V shapes formed by preferential etching. The TEM measurements were conducted at the apex of these V shapes with confidence that these areas corresponded to shear bands. We note that the edge of the perforation for the as-spun specimen was smooth, in contrast to the deformed specimens. When examining the deformed specimens in the TEM we did not observe an extremely abrupt contrast difference between
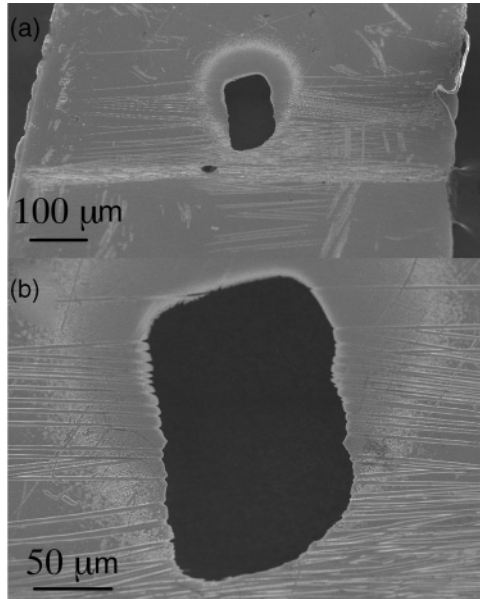
FIG. 3. SEM images of a typical deformed TEM specimen. (a) The perforation has formed in the network of shear steps near the bend. (b) The shear bands have etched preferentially, and their position around the perforation is evident.

shear bands of 10–20 nm in size,[22] and the surrounding matrix. The only contrast difference we observed was consistent with a gradual change in projected thickness due to preferential etching occurring in the micron range, as we see in Fig. 3. This preferential etching may be due to a structural difference between the shear band and the matrix, or due to the existence of a surface step at the shear band.[8] The lack of an abrupt difference in contrast indicates that the difference between the structure of the shear band and the matrix is subtle, supporting the quantitative techniques pursued in this study.

Figures 4(a), 4(c), and 4(e) show phase contrast images of the as-spun specimen and specimens deformed in compression and tension. The corresponding projected thickness maps reconstructed using Eq. (1) are shown in Figs. 4(b), 4(d), and 4(f). The profiles across these surfaces [Fig. 4(g)] demonstrate that we generally have wedge-shaped specimens. The small variations in projected thickness correspond to real variations due to surface features or internal voids. The results we present now are the average of six to eight specimen regions per specimen, depending on how many suitable regions each specimen presented. We confined our analysis to regions with a projected thickness of ~20 nm, as this was thickness that was observed most consistently. We will discuss the impact this has on resolution in a subsequent section.

To quantify differences in the variations in the projected thickness between the as-spun and deformed glasses, we calculated the azimuthally averaged autocorrelation functions of the projected thickness maps. The projected thickness maps were high-pass filtered to remove the ramp in the autocorrelation due to the wedge-shaped specimen but retain the high-frequency information from voids. The autocorrelation function was calculated using the Wiener-Khinchin theorem.[23]

In Fig. 5(a) we show a simulated projected thickness map from a void field in a flat, parallel-sided specimen
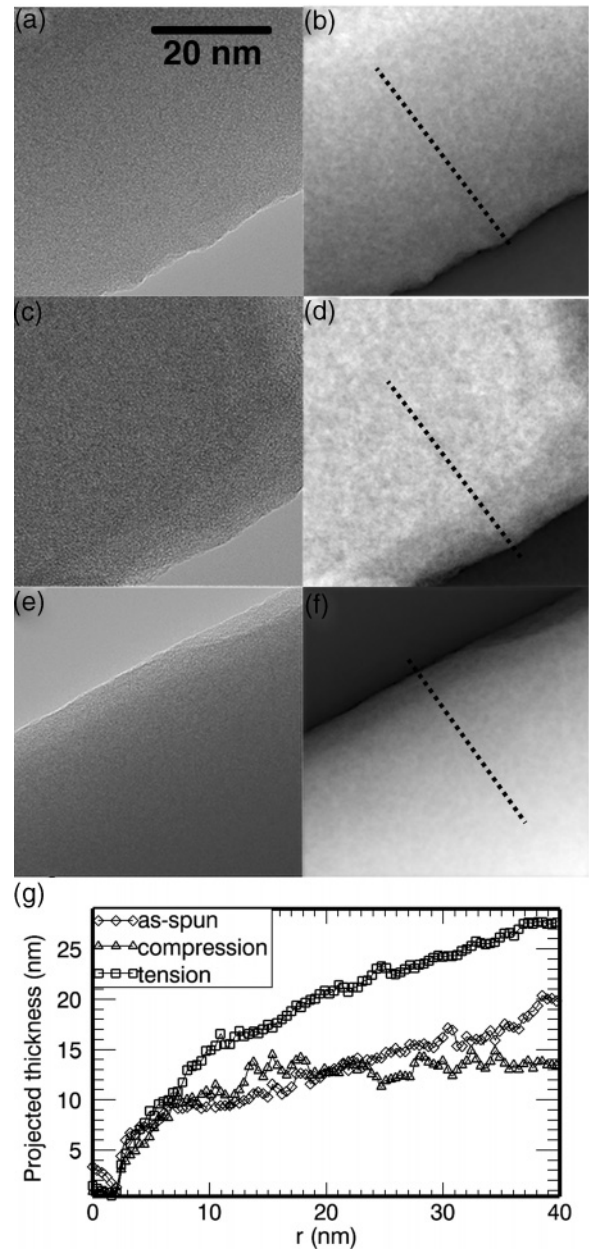

FIG. 4. Phase contrast images from the (a) as-spun glass and glasses deformed in (c) compression and (e) tension. (b), (d), and (f) Corresponding reconstructed projected thickness maps from these phase contrast images. (g) Profiles through the projected thickness maps from the dashed lines indicated.

with a 0.025 volume fraction of voids of 1 nm in radius. In Fig. 5(b) we display the simulated phase contrast image from this object using the identical instrumental and material parameters to this experiment.[24] Note that the scale of these images is almost identical to the scale of the images and reconstructed projected thickness maps from the data (Fig. 4). In Fig. 5(c) we display the corresponding autocorrelation function calculated for this simulated void field. We also display an autocorrelation function calculated for a random void field (0.025 volume fraction of 2-nm radius voids) and a semirandom void field (0.025 volume fraction of 1-nm radius voids) in which the voids are randomly placed within their
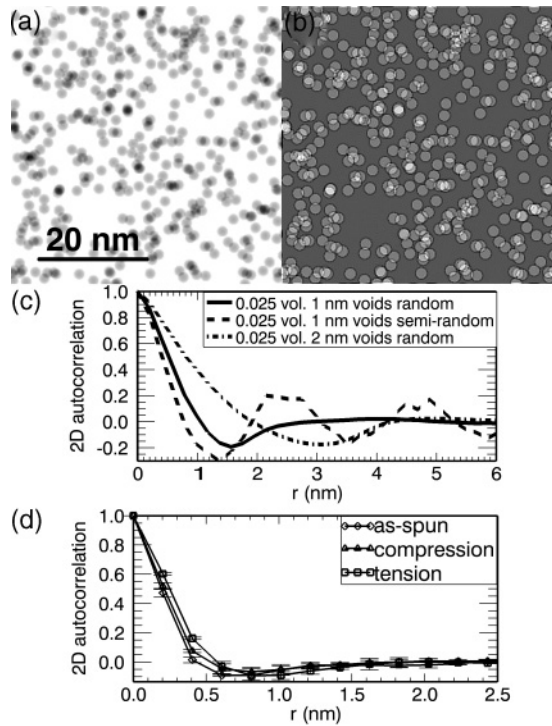
FIG. 5. (a) Simulated projected thickness map from a void field in a parallel-sided specimen with 0.025 volume fraction of 1-nm radius voids randomly placed. (b) Simulated phase contrast image from this specimen using the same instrumental parameters as this study. The scale of these images is almost identical to the scale of the images and reconstructed projected thickness maps shown in Fig. 4. Azimuthally averaged autocorrelation functions of projected thickness from (c) simulated void fields and (d) the as-spun and deformed $Zr_{66.7}Cu_{33.3}$ glass.
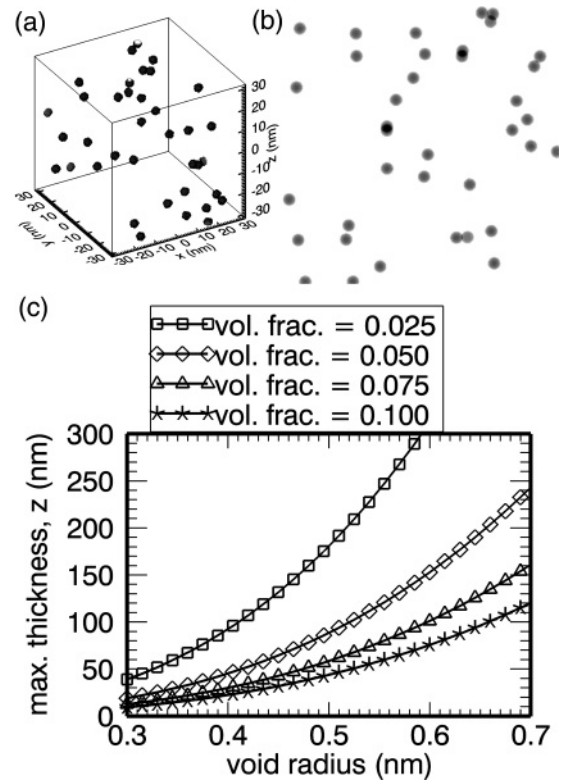

FIG. 6. Simulated void field (1.5-nm radius and 0.002 fraction by volume) displayed as a volume (a) and in projection (b). (c) Maximum thickness of specimen to resolve voids of a given radius and volume fraction.

own projected area (not shown). For the randomly placed void fields the autocorrelation function passes through zero at the radius of the voids, then exhibits a small anticorrelation, due to the low incidence of void overlap, and finally oscillates with small amplitude around zero at larger distances as correlations average to zero. If the voids are semirandomly placed, the autocorrelation has additional peaks corresponding to average first and second nearest neighbor intervoid distances. Surface features with a characteristic size will also give rise to features in the autocorrelation function. However, we note that electropolishing artifacts are typically >20 nm in size[25], and thus such surface features won't interfere with our analysis.

Examining the autocorrelation functions from the projected thickness maps of the as-spun glasses and the shear bands formed in compression and tension [Fig. 5(d)], we see they are equal within error across almost the entire distance range. There is a small discrepancy at 0.4 nm, with the glass deformed in tension having a larger correlation than the other specimens. However, this difference is too close to the technique resolution limit of 0.32 nm to confidently assert a structural difference between the glasses in terms of differences in the projected thickness. Voids of 1-nm radius could be detected, as they would be sampled four times in the autocorrelation function at this resolution.

When examining an assembly of random objects in projection the size of the objects that can be resolved depends on both the resolution of the technique and the size and number density of the objects.[26] This is demonstrated in Fig. 6 which shows a population of 1.5-nm radius voids at a volume fraction of 0.002 as a volume (a) and in projection (b). In the projection, lengths smaller than the void diameter exist, due to overlap between the voids. If the voids are extremely dense, the detail in the projection will be smaller than the technique resolution, and the voids will not be resolved, even if their size is larger than the resolution.

We can determine the maximum thickness of a specimen to resolve voids of a given radius, r_{void}, and at a given volume fraction v_{frac}.[26] The areal number density of voids is $A = N \times z$ where N is the volume number density, and z is the specimen thickness. The average distance, l, between voids in the projection is given by $A \approx 1/\pi(l/2)^2$. Equating these two expressions we find $z \approx 4/\pi l^2 N$. In order to resolve the voids we require that l be greater than twice the resolution, ρ. Thus, $z \leqslant 1/\pi\rho^2 N$. For a given volume fraction and diameter, $N = v_{frac}/(\frac{4}{3}\pi r_{void}^3)$. In Fig. 6(c) we plot this maximum thickness as a function of void radius for volume fractions between 0.025–0.1. Examining this figure we can assess the real resolution limits of this technique. We see that employing a specimen thicknesses of 20 nm, voids with a radius of 0.32 nm at the limit of the technique resolution, can be resolved if they exist at a volume fraction of 0.075 or below. Smaller and denser populations of voids will not be detected. However, we note that a volume fraction of 0.075 would equate to a density deficit in the shear band of 7.5%, which would give rise to a more

pronounced mass-thickness contrast difference in the original phase contrast images than we have observed ($\sim$3.5% with a 7.5% reduction of μ at 20 nm).

Atomic modeling studies employing molecular dynamics examining both Zr_xCu_{100-x} glasses[27,28] and ideal binary glasses[29,30] have found that atomic volume increases in regions of shear localization and plastic deformation. One study found evidence of voids in the crater morphology of a crack surface.[27] However, others have reported that the density fluctuations cannot be resolved on the length scale of the shear band above the fluctuations inherent in the glass structure[29], or that the open volumes with a roughly spherical morphology were below 0.6 Å in size.[28] These modeling studies and bulk positron annihilation spectroscopy measurements[6] are consistent with the conclusions of our microscopic measurement, and suggest that the free volume evolved during inhomogeneous deformation does not condense into large spherical voids, but is distributed more diffusely. Based upon the number of shear bands and the overall, bulk density reduction, and assuming all the free volume is localized in shear bands, one may expect that the shear bands will have a density deficit of $>$10%.[5] This is not consistent with the size of the free volume accumulations found in this study. A recent indentation study of an inhomogeneously deformed Zr-based glass found that both the shear band and intershear band material displayed a reduced hardness with respect to undeformed material.[31] This also suggests that the free volume formed during inhomogeneous deformation is distributed and diffuse.

Dilatation confined to shear bands during deformation of granular materials such as sand has been well documented.[32] Full-field x-ray attenuation measurements on macroscopic specimens show planes of density deficit of 2–4 mm without complications in interpretation from specimen preparation.[32] Thin sections taken perpendicular to the shear band have been examined by optical microscopy in which the 100–200-μm diameter particles could be clearly resolved. In the shear band the void ratio (defined as the free space area normalized by the area covered by particles[33]) was found to be elevated with respect to the matrix (1.01 compared to 0.69). Voids were also detected in the shear band with radii of $\sim$100 μm, corresponding to one to eight particle volumes, given the distribution of grain sizes. In granular materials thermal motion is small compared to particle size, and there are no cohesive forces between particles. Yet even in these systems the void volume in shear bands is at most eight times the particle volume. In our random atomic system, we detect no voids down to a resolution of 20 atomic volumes. In light of the findings on granular systems, this limit on void size seems entirely consistent.

The resolution of our technique is limited by an approximate expansion of the complex contrast transfer function of the microscope, an expansion which is only valid up to a certain spatial frequency, for a given set of instrument parameters.[16] It is possible that smaller voids might be detected using a higher resolution technique, for example, with multiple phase contrast images. However, beyond 0.3 nm the single-material object assumption loses meaning, as the atomicity of the material must be taken into account, strongly suggesting that a technique sensitive to atomic arrangements needs to be pursued to investigate the structure of shear bands. Modeling studies have also demonstrated large changes to the short- and medium-range atomic order of glasses due to deformation,[29,30] suggesting that a technique such as fluctuation electron microscopy,[34] which probes medium-range order, should be pursued.

IV. CONCLUSIONS

Our quantitative microscopic measurement of the distribution of voids in shear bands using a medium-resolution phase retrieval technique indicates that voids of larger than 0.32 nm in radius (corresponding to 20 atomic volumes) are not present in the shear bands of deformed glasses. This places a useful upper limit on the size of free volume accumulations in regions of shear localization in glasses and also indicates that larger voids are not energetically stable in these random, cohesive atomic systems. Our findings are consistent with bulk positron annihilation spectroscopy measurements[6] and many modeling studies[28–30], and demonstrate that the free volume created during inhomogeneous deformation is distributed more diffusely, and does not condense into larger volumes. If the free volume does condense uniformly into larger nm-sized voids in shear bands, this might be a transient effect. Likewise, the free volume generated within the shear band may dissipate after the shear front has passed, or once the load has been removed. We anticipate that this single-image technique will be ideal for monitoring such dynamic effects, for example, in an *in situ* deformation experiment.

*amelia.liu@monash.edu

[1]D. Turnbull and M. H. Cohen, J. Chem. Phys. **52**, 3038 (1970).

[2]A. V. den Beukal and S. Radelaar, Acta Metall. **31**, 419 (1983).

[3]F. Spaepen, Acta Metall. **25**, 407 (1977).

[4]D. Deng and B. Lu, Scr. Metall. **17**, 515 (1983).

[5]C. A. Schuh, T. C. Hufnagel, and U. Ramamurty, Acta Mater. **55**, 4067 (2007).

[6]K. M. Flores, E. Sherer, A. Bharathula, H. Chen, and Y. Jean, Acta Mater. **55**, 3403 (2007).

[7]J. Li, Z. L. Wang, and T. C. Hufnagel, Phys. Rev. B **65**, 144201 (2002).

[8]P. E. Donovan and W. M. Stobbs, Acta Metall. **29**, 1419 (1981).

[9]W. H. Jiang and M. Atzmon, Acta Mater. **51**, 4095 (2003).

[10]W. J. Wright, T. C. Hufnagel, and W. D. Nix, J. Appl. Phys. **93**, 1432 (2003).

[11]K. Nagayama, Eur. Biophys. J. **37**, 345 (2008).

[12]J. N. Chapman, A. B. Johnston, and L. J. Heyderman, J. Appl. Phys. **76**, 5349 (1994).

[13]W. O. Saxton, *Computer Techniques for Image Processing in Electron Microscopy* (Academic Press, New York, 1978).

[14]Y. M. Chen, T. Ohkubo, T. Makai, and K. Hono, J. Mater. Res. **24**, 1 (2009).

[15]D. Paganin, S. C. Mayo, T. E. Gureyev, P. R. Miller, and S. W. Wilkins, J. Microsc. **206**, 33 (2002).

[16]A. C. Y. Liu, D. M. Paganin, L. Bourgeois, and P. N. H. Nakashima, Ultramicroscopy **111**, 959 (2011).

[17]F. M. Ross and W. M. Stobbs, Philos. Mag. A **63**, 37 (1991).

[18]N. Mattern, A. Schöps, U. Kühn, J. Acker, O. Khvostikova, and J. Eckert, J. Non-Cryst. Solids **354**, 1054 (2008).

[19]P. N. H. Nakashima and A. W. S. Johnson, Ultramicroscopy **94**, 135 (2003).

[20]J. M. Cowley, *Diffraction Physics*, 3rd ed. (North-Holland, Amsterdam, 1995).

[21]A. C. Y. Liu, R. Arenal, D. J. Miller, X. Chen, J. A. Johnson, O. L. Eryilmaz, A. Erdemir, and J. B. Woodford, Phys. Rev. B **75**, 205402 (2007).

[22]Y. Zhang and A. L. Greer, Appl. Phys. Lett. **89**, 071907 (2006).

[23]R. N. Bracewell, *The Fourier Transform and Its Applications*, 2nd ed. (McGraw-Hill, New York, 1986).

[24]E. J. Kirkland, *Advanced Computing in Electron Microscopy* (Plenum Press, New York, 1998).

[25]D. Nagahama, T. Ohkubo, and K. Hono, Scr. Metall. **49**, 729 (2003).

[26]D. V. Dyck, S. V. Aert, A. J. den Dekker, and A. van den Bos, Ultramicroscopy **98**, 27 (2003).

[27]Q.-K. Li and M. Li, Phys. Rev. B **75**, 094101 (2007).

[28]M. I. Mendelev, R. T. Ott, M. Heggen, M. J. Kramer, and D. J. Sordelet, J. Appl. Phys. **104**, 123532 (2008).

[29]Y. Shi and M. L. Falk, Scr. Mater. **54**, 381 (2006).

[30]F. Albano and M. L. Falk, J. Chem. Phys. **122**, 154508 (2005).

[31]B.-G. Yoo, Y.-J. Kim, J.-H. Oh, U. Ramamurty, and J.-L. Jang, Scr. Mater. **61**, 951 (2009).

[32]M. Oda and H. Kazama, Géotechnique **48**, 465 (1998).

[33]J. P. Bardet and J. Proubel, Géotechnique **41**, 599 (1991).

[34]M. M. J. Treacy, J. M. Gibson, L. Fan, D. J. Paterson, and I. McNulty, Rep. Prog. Phys. **68**, 2899 (2005).